Polymer 49 (2008) 4433–4445

Contents lists available at ScienceDirect

Polymer

journal homepage: www.elsevier.com/locate/polymer

Defining the physical structure and properties in novel monofilaments with potential for use as absorbable surgical sutures based on a lactide containing block terpolymer

Wasinee Channuan [a], Jintana Siripitayananon [a], Robert Molloy [a], Geoffrey R. Mitchell [b,*]

[a] Biomedical Polymers Technology Unit, Department of Chemistry, Faculty of Science, Chiang Mai University, Chiang Mai 50200, Thailand
[b] Centre for Advanced Microscopy and Polymer Science Centre, University of Reading, Reading RG6 6AF, UK

ARTICLE INFO

Article history:
Received 10 January 2008
Received in revised form 27 April 2008
Accepted 24 July 2008
Available online 5 August 2008

Keywords:
Block terpolymer
Fibre
Morphology

ABSTRACT

Monofilaments of a block terpolymer of L-lactide, ε-caprolactone and glycolide have been melt spun for potential use as absorbable surgical sutures. As-spun fibres of the terpolymers produced by melt spinning were elastic, amorphous and isotropic. A two-stage process involving hot drawing was employed to enhance their mechanical properties. WAXS and SAXS results coupled with DSC demonstrated that hot drawing leads to an orientated amorphous matrix containing small highly aligned crystals. Hot drawing was carried out at a range of temperatures using the highest possible draw rate commensurate with maintaining continuity of the fibre. A novel WAXS analysis based on a spherical harmonic analysis allowed a separation of the scattering into three components: oriented crystalline, oriented amorphous, and an isotropic amorphous. There is a steady increase in the fraction of oriented crystalline material with increasing hot draw temperature, although the level of crystallinity is ultimately limited by the statistical nature of the terpolymer. The material shows highly promising potential properties for use as a monofilament suture.

1. Introduction

The use of polymer-based monofilaments as absorbable sutures in internal surgery applications places considerable demands on the physical properties [1,2]. The smoothness of monofilaments in contrast to multi-filaments braids minimize the drag within the tissue and associated effects such as sawing. The filament itself needs to be both pliable and sufficiently strong to enable knot tying, while a high level of crystallinity will slow the absorption rate. The development of suitable materials requires careful selection of the chemical configuration as well as the filament processing conditions. Among all resorbable biomaterials, copolymers and terpolymers of L-lactide, glycolide and ε-caprolactone appear to be the most attractive in biocompatible applications. The broad expectation that materials prepared from these components will be biocompatible has been widely established by others [3] for example, detailed biocompatibility studies on copolymers of lactide and glycolide [4] and copolymers of glycolide and caprolactone [5]. The commercial suture Monocryl (Johnson & Johnson) is based on a random copolymer of 75% glycolide and 25% caprolactone [5]. Such commercial sutures are semi-crystalline with a high level of preferred crystal orientation. The mechanical properties are determined by the quantitative detail of the semi-crystal morphology and this is in turn defined by the processing conditions.

We have set out to provide control of these properties through the use of a block terpolymer configuration which contains a non-crystallisable core based on L-lactide-*co*-ε-caprolactone which remains flexible [6]. The terminal blocks are formed from L-lactide-*co*-glycolide. The fraction of glycolide is small allowing sufficient scope for the all important crystallisation of the L-lactide units. This approach, based on terpolymers allows the properties to be tuned by variation in copolymer structure and composition. Here, the design combines the potential mechanical strength of L-lactide with the chain flexibility of ε-caprolactone and enhanced biodegradability of the glycolide. Furthermore, the use of appropriate terpolymers facilitates lower processing temperatures which benefit polymer stability and minimises degradation products. We have developed a two-stage processing route to allow optimisation of properties within the laboratory environment. The initial stage involves the preparation of monofilaments which are amorphous and isotropic. The final properties are defined through a hot drawing stage. We have previously shown that this novel block terpolymer develops a significant level of crystallinity in which the crystals are formed from the lactide sequences in a structure essentially equivalent to that of hot drawn fibres of polylactide [7]. In this work, we have used wide-angle and small-angle X-ray

* Corresponding author. Tel.: +44 118 3788573; fax: +44 118 9750203.
E-mail address: g.r.mitchell@reading.ac.uk (G.R. Mitchell).

0032-3861/$ – see front matter © 2008 Elsevier Ltd. All rights reserved.
doi:10.1016/j.polymer.2008.07.058

scattering procedures together with mechanical testing to explore the processing-structure–property relationships in order to identify the optimum processing conditions required to yield fibres with the required properties.

2. Experimental

2.1. Materials

All of the work reported here was performed using a block terpolymer (Fig. 1) with the structure poly[(L-lactide-*co*-glycolide)-*b*-(L-lactide-*co*-ε-caprolactone)-*b*-(L-lactide-*co*-glycolide)]. The terpolymer was synthesized using a methodology which involves first forming the central block and then secondly the terminal blocks [8,9]. ^{1}H NMR revealed an overall composition of 71% lactide, 25% ε-caprolactone, 4% glycolide. More detailed analysis of the ^{1}H and ^{13}C NMR spectra gave a lactide sequence length of ~8 which translates into a sequence length of ~10 for the outer blocks, if the central block is a random mixture of LL and CL [7]. The final polymer had an inherent viscosity of 0.98 dl/g at 30 °C in chloroform and through GPC in tetrahydrofuran, a M_w of 47,000 and M_w/M_n of 1.71. The block terpolymer was cut into small pieces, dried in vacuo and then these small pieces were used as the feedstock for the small-scale fibre spinning process.

2.2. Preparation of terpolymer fibres

Fibres were produced by a two-stage (melt spinning and hot drawing) process. "As-spun" fibres, which were optically clear, were prepared using small-scale (5–10 g) melt spinning apparatus (Ventures & Consultancy Bradford Ltd. UK) equipped with a single hole spinneret of diameter 1.0 mm. An extrusion rate of 0.10 mm/min was used with an extruder barrel of 16.0 mm diameter and a temperature of 167 °C. The extruded fibre was quenched in to an ice-water bath with take up rate of 1.0 m/min. As-spun fibres were subsequently hot drawn with a range of draw rates at various temperatures from 30 to 80 °C.

There are several interrelated parameters which will define the subsequent structure and morphology. From preliminary work on these block copolymer fibres and from the general literature [10], it is clear that the draw rate is a strong controlling factor for the subsequent structure and morphology. In particular, a higher draw rate is expected to produce a greater degree of preferred orientation in the amorphous matrix. We selected to draw the fibres at the fastest rate commensurate with maintaining continuity of the fibre. Each as-spun fibre was held for 30 s in the hot drawing unit at the selected temperature and then drawn with a defined draw rate. The average draw ratio obtained for ~5 fibres prepared in this manner and the draw rates used are shown in Table 1. It was not possible to draw samples at temperatures above 80 °C using this approach. As can be seen from the figures in the table there is approximately a linear relationship between the temperature and draw ratio. This set of experiments is effectively performed at points along the line in temperature–draw rate space which divides the space into drawable and undrawable. At each of these points we have selected to extend the fibre to the maximum draw ratio possible without breakage. We anticipate that these conditions will produce fibres with the greatest preferred molecular orientation in the amorphous phase for a given temperature.

Table 1
Average draw ratio and draw conditions for off-line hot drawing at various temperatures

Polymer	$T_{drawing}$ (°C)	Draw rate (%/min)	Draw ratio
Block terpolymer	30	860	3.9
	40	1020	4.6
	50	1780	5.4
	60	3040	7.0
	70	5280	7.5
	80	4480	9.4

2.3. Thermal properties

Thermal properties were measured under flowing nitrogen atmosphere in a Perkin–Elmer DSC-7 calibrated with indium and were conducted at a heating rate of 5 °C/min in the range of 25–250 °C. Each sample of 3–5 mg was prepared by winding the fibre around a piece of aluminum and then mounted in a standard sample pan.

2.4. Wide-angle X-ray scattering (WAXS)

Wide-angle X-ray scattering measurements on the final filaments at room temperatures were made using a symmetrical transmission diffractometer equipped with a graphite monochromator and pinhole collimation together with a Cu source shown schematically in Fig. 2. The intensity values from isotropic samples were obtained as a function of $|\underline{Q}|$ over the range

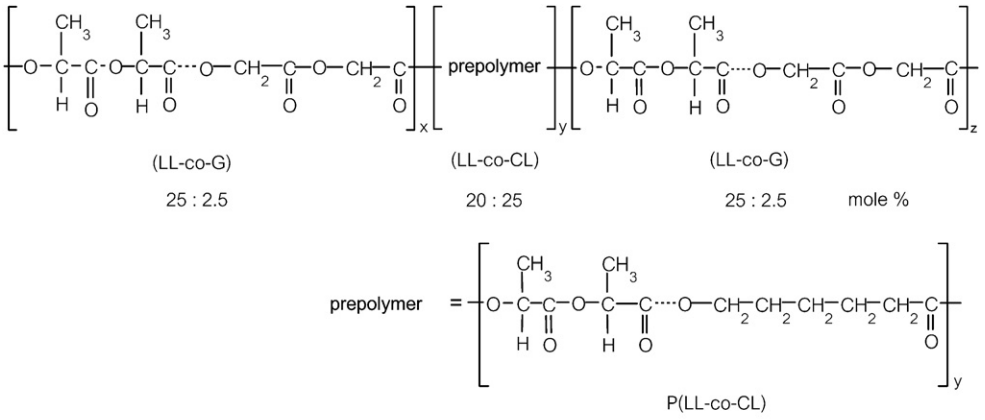

Fig. 1. Chemical structure of the block terpolymer used in this work.

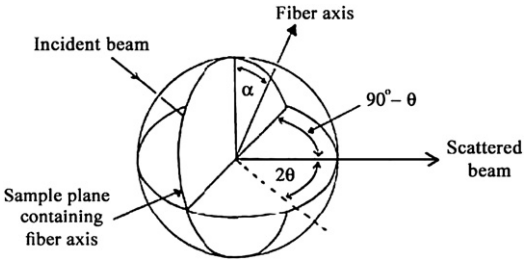

Fig. 2. Schematic of the geometry of the 3-circle X-ray diffractometer used in this work.

0.2–6 Å^{-1} in steps of 0.02 Å^{-1} where $|\underline{Q}| = 4\pi \sin\theta/\lambda$, 2θ is the scattering angle and λ is the incident X-ray wavelength. Data for anisotropic samples were obtained as a function of $|\underline{Q}|$ over the range 0.2–6 Å^{-1} in steps of 0.02 Å^{-1} and α over the range 0°–90° in steps of 2°. α is the angle between the symmetry axis of the sample and the scattering vector $|\underline{Q}|$. The situation when $\alpha = 0°$ corresponds to the meridional section, parallel to the fibre axis and $\alpha = 90°$ corresponds to the equatorial section. Specimens were prepared by mounting a parallel array of closely packed filaments. In this arrangement the X-ray beam typically intercepts 2–3 fibres. The scattering data were corrected for the effects of absorption, polarization, multiple and incoherent scattering and scaled to absolute units using standard procedures [11].

2.5. Small-angle X-ray scattering

Small-angle X-ray scattering (SAXS) data were obtained on the fixed wavelength ($\lambda = 1.4$ Å) beam-line 16.1 at the Daresbury Synchrotron Radiation Source (UK) using a sample to detector distance of ~3 m and a beam ~0.3 mm diameter. The SAXS data were recorded using a 2-D RAPID detector calibrated in terms of geometry using a collagen sample. The intensity data were normalized to the incident beam using the values obtained from an ionization chamber prior to the sample.

2.6. Mechanical properties

Tensile properties of the terpolymer fibres were measured at ambient temperature (22–25 °C) using a Lloyds LRX+ Universal Testing Machine with a 100 N load cell, at a crosshead speed of 20 mm/min. The initial gauge length of each specimen was 40 mm and the fibre diameter was measured to the accuracy of ±0.001 mm.

3. Results

3.1. Thermal properties by DSC

Characterization of the starting material by DSC at a heating rate of 20 °C/min gave $T_m \sim 156$ °C ($\Delta H_m = 25.2$ J/g) and $T_g \sim 42$ °C. Fig. 3 shows the results of the thermal analysis, in terms of the temperature at the peak in the melting endotherm, for the series of fibres shown in Table 1. There is a small increase in the observed melting peak temperature with draw temperature suggesting that the crystal thickness is largely but not completely constant. For comparison, the melting point of the homopolymer of poly(L-lactide) is reported to be in the range 170–180 °C [12]. Two factors are significant in terms of the crystal thickness. The first is the random copolymer nature of the crystallizing lactide dominant terminal blocks and hence the limit on the possible crystal thickness through the chemical disorder. The second is that crystallization was induced by hot drawing at a high rate and therefore only a very short time was available for the crystallization process.

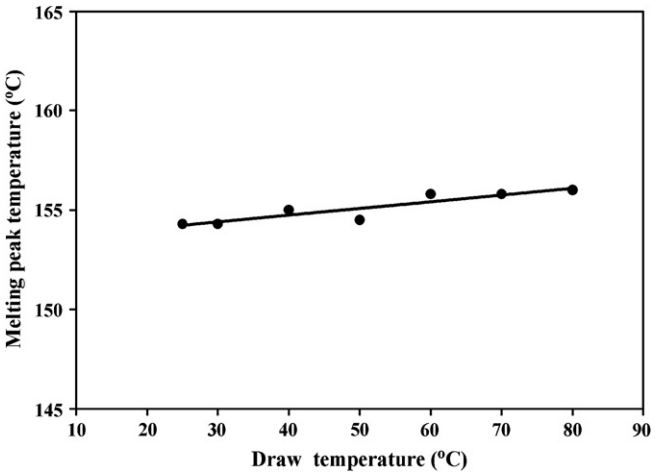

Fig. 3. Plot of the melting peak temperature, T_m, against the draw temperature (full draw conditions are given in Table 1) used to prepare each of the block terpolymer fibers.

The fibres prepared at 30 °C and 40 °C showed a small amount of cold crystallization upon heating in the DSC while those prepared at higher temperatures exhibited no significant cold crystallization. We used the DSC curves to calculate the level of crystallinity in each fibre by evaluating the fusion enthalpy and subtracting from it the corresponding crystallization enthalpy for cases where cold crystallization had occurred. Fig. 4 shows the results of these calculations. We plot the measured differences between the heat of melting (ΔH_m) and the heat of crystallization (ΔH_c) for the series of fibres prepared under different conditions (Table 1). $\Delta H_m - \Delta H_c$ is a measure of the crystalline content in each fibre. The values of $\Delta H_m - \Delta H_c$ indicate that the crystallinity increases with draw ratio and a maximum value of $\Delta H_m - \Delta H_c \approx 25$ J/g is observed for the sample prepared at the highest temperature and draw ratio. Turner et al. [13] reported a value of 93.6 J/g for ΔH for 100% crystalline poly(L-lactide) phase. Although the situation considered here with the crystals embedded in an amorphous matrix made up of the central block and non-crystallised terminal blocks is not exactly the same as the homopolymer, it is useful to use this value to scale the observations to give the fraction of crystalline material and these are also shown in Fig. 4.

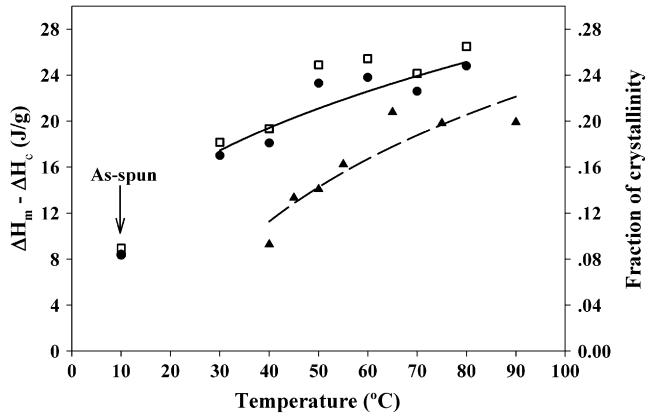

Fig. 4. Plot of $\Delta H_m - \Delta H_c$ (●) and fraction of crystallinity (□) against the drawing temperature used to prepare each block terpolymer fibers (full drawing conditions are given in Table 1). The filled triangles (▲) show the measured crystallinity for a series of samples of the block terpolymer isothermally crystallized under quiescent conditions at the indicated temperatures.

The scaling suggests a maximum crystalline fraction of ~0.26. Turner et al. report a reduction of crystallinity for poly(L-lactide) fibres with draw ratios >4, however, the draw rates used were constant with increasing temperature in contrast to the increasing rates used in this work [13]. In Fig. 4 we have also presented the fraction of crystalline material for samples crystallized under quiescent conditions at the same series of temperatures used to prepare the fibres. It is clear that there is a significant increase in the level of crystallinity in the drawn samples compared to the samples crystallized without drawing at the same temperature. The change equates to a horizontal shift in the curves by ~30 °C. The slightly lower slope of the crystallinity versus temperature curve for the fibres, suggests that the material may be approaching the limit of crystallinity defined by the random copolymer nature of the 'crystallisable' end blocks.

3.2. Structure characterization

Fig. 5 shows the wide-angle X-ray scattering patterns recorded for the as-spun fibre and for fibres drawn under the various conditions shown in Table 1. Although these X-ray patterns have the appearance of simple diffraction patterns taken with a flat area detector, such as an image plate, it is emphasized that these are undistorted maps of reciprocal space obtained with a diffractometer. The full-map of reciprocal space enables the detailed orientational analysis which is described later. To facilitate the presentation of the essential features, the scattering data is shown in grey-scale form over the restricted range of $|\underline{Q}| = 0$–$3\ \text{Å}^{-1}$ and $\alpha = 0$–90°. The as-spun filament (Fig. 5a) shows a largely isotropic pattern with very diffuse peaks centered at $|\underline{Q}| = 1.2$ and $2.1\ \text{Å}^{-1}$. The remaining patterns, Fig. 5b–g show the X-ray scattering patterns for the drawn filaments. The scattering in each of these patterns is clearly anisotropic indicating that there is a significant level of preferred orientation of the structural correlations present in these filaments. Fig. 5b shows the pattern obtained from fibres drawn at 30 °C, which exhibits an anisotropic but rather diffuse peak which is overlaid with a more intense and sharper feature (both radially and equatorially) localized on the equator at $|\underline{Q}| = 1.16\ \text{Å}^{-1}$. There is a feature which is most intense on the meridian at $|\underline{Q}| = 2.18\ \text{Å}^{-1}$. As we move through the series of patterns corresponding to increasing draw temperatures, the rather broad and diffuse feature becomes more anisotropic but equally reduces in intensity such that it is hardly visible in the last pattern shown in Fig. 5g for fibres drawn at 80 °C. At the same time the more distinctive features at 1.16 and $2.14\ \text{Å}^{-1}$ become more intense and sharper. These correspond to almost perfectly aligned crystals. It is striking that, even with this rather disordered terpolymer, a modest draw ratio leads to highly aligned crystals in the same manner as for stretched rubber [14] or fibres of the homopolymer [15].

Fig. 6 shows the intensity profiles along the equatorial ($\alpha = 90$) and meridional ($\alpha = 0$) directions for the WAXS pattern shown in Fig. 5 plotted as a function of $|\underline{Q}|$. The changing shape of both the equatorial and meridional peaks can be easily seen. The values of $|\underline{Q}|$ corresponding to the maxima can be converted to an apparent interplanar spacing (d) using:

$$d = \frac{2\pi}{|\underline{Q}|_0} \tag{1}$$

where $|\underline{Q}|_0$ is the peak position. The correlation length or effectively the crystal width, can be determined from the width of the peak at half-height width ($\Delta|\underline{Q}|$):

$$l_c = \frac{2\pi}{|\Delta\underline{Q}|} \tag{2}$$

The results of the application of these two equations to the peaks observed in the equatorial and meridional sections (Fig. 6) are shown in Fig. 7a and b. The peak positions are more or less constant. There is a small shift downwards in the position of the equatorial peak and a small shift upwards for the meridional peak with increasing draw temperature. We attribute these modest changes to the increasing influence of the crystalline component in each case on the overall peak position.

The measurements of the widths of the equatorial and meridional peaks have been converted to correlation lengths using Eq. (2) and the results are plotted in Fig. 7b. There is an increase in the correlation length in the direction parallel to the fibre axis and we attribute this to an increase in the crystal thickness which parallels the increase in the melting peak temperature with increasing draw temperature shown in Fig. 3. As identified above, any increase in crystal thickness is ultimately limited by the random nature of the copolymer terminal blocks. NMR measurements showed that the typical lactide run length is of the order of 10 lactide units or ~60 Å. Clearly, this would be the maximum crystal thickness if all terminal blocks were of the same length and with the same monomer distribution. The statistical nature of the copolymer blocks means that the 40 Å thickness observed is probably approaching the upper limit. The correlation length in the equatorial direction increases more substantially with increasing draw temperature as would be expected for a system with a higher level of crystallinity. Similar results were reported by Fu et al. for random copolymers of lactide and glycolide [16].

3.3. Orientation

The series of wide-angle X-ray scattering patterns shown in Fig. 5 exhibit both diffuse and sharp features characteristic of a structure with both amorphous and crystalline components. Closer examination of the patterns shows that both components exhibit anisotropy. It is relatively straightforward to evaluate the anisotropy in the scattering pattern by considering the azimuthal variation of the intensity at a constant value of $|\underline{Q}|$. Fig. 8 shows the normalized azimuthal variation in intensity at $|\underline{Q}| = 1.16\ \text{Å}^{-1}$ for each fibre. The as-spun fibre shows a constant level of intensity underlining the isotropic nature of the structure, while the drawn fibres exhibit a varying level of azimuthal variation. Each shows maxima at 90° and 270° indicating the equatorial nature of the maxima. There are a variety of approaches to quantify the level of anisotropy. We prefer the unambiguous definition based on the analysis of the scattering pattern in terms of spherical harmonics [17,18].

The scattering intensity data, $I(|\underline{Q}|, \alpha)$, of each diffraction pattern as shown in Fig. 5 was expressed as a series of spherical harmonics, $I_{2n}(|\underline{Q}|)$:

$$I_{2n}(|\underline{Q}|) = (4n+1)\int_0^{\pi/2} I(|\underline{Q}|, \alpha) P_{2n}(\cos\alpha)\sin\alpha \mathrm{d}\alpha \tag{3}$$

where $P_{2n}(\cos\alpha)$ are Legendre polynomials; only even numbered terms are required due to the inversion symmetry inherent in an X-ray diffraction pattern for a non-absorbing sample. The complete scattering pattern may be calculated from the weighted sum of these harmonics:

$$I(|\underline{Q}|, \alpha) = \sum_{2n=0}^{\infty} I_{2n}(|\underline{Q}|) P_{2n}(\cos\alpha) \tag{4}$$

In this work, the first five spherical harmonic components (I_0, I_2, I_4, I_6 and I_8) obtained for each sample are shown in Fig. 9. I_0 represents the scattering from an equivalent macroscopically unoriented sample, while I_2, I_4, I_6, I_8, … I_{2n} arise from the anisotropic scattering,

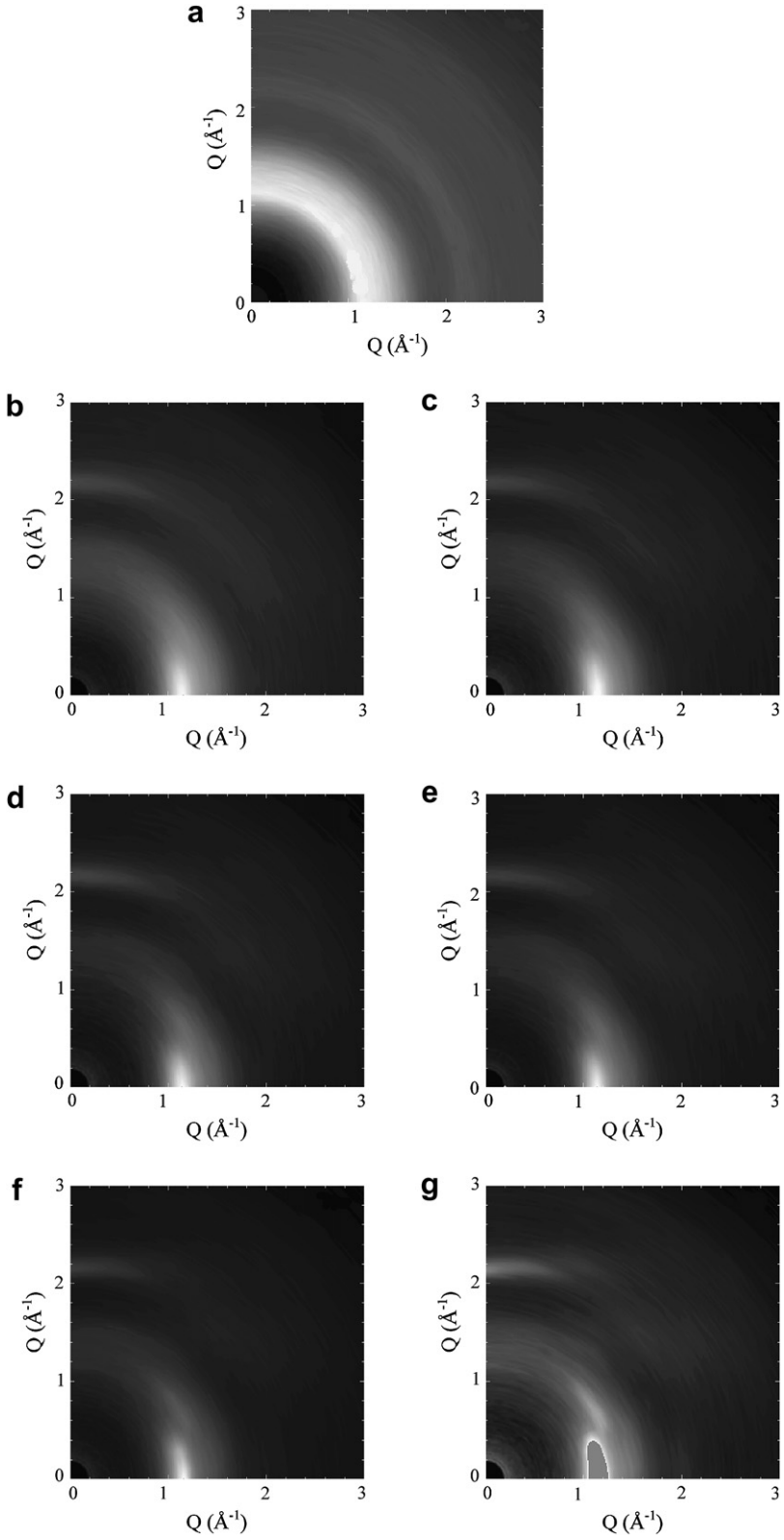

Fig. 5. Wide-angle X-ray diffraction patterns of the block terpolymer fibres drawn under various conditions: (a) as-spun fibre; (b) $T = 30\,^{\circ}C$; (c) $T = 40\,^{\circ}C$; (d) $T = 50\,^{\circ}C$; (e) $T = 60\,^{\circ}C$; (f) $T = 70\,^{\circ}C$ and (g) $T = 80\,^{\circ}C$. Full draw conditions are given in Table 1. The fibre axis is vertical on the page.

which may well include scattering from both crystalline and amorphous phases.

Inspection of the series of spherical harmonics for example Fig. 9e reveals some interesting characteristics. The I_0 curve has a very broad peak while that for I_8 appears to be quite sharp. The I_2 curve has the sharpness of the I_8 curve but has an additional shoulder at higher $|\underline{Q}|$ but the overall peak is not as broad as the I_0 function. Clearly the fibre contains differing structural components. Similar observations can be made about each set of harmonics although the balance between the strength of any component

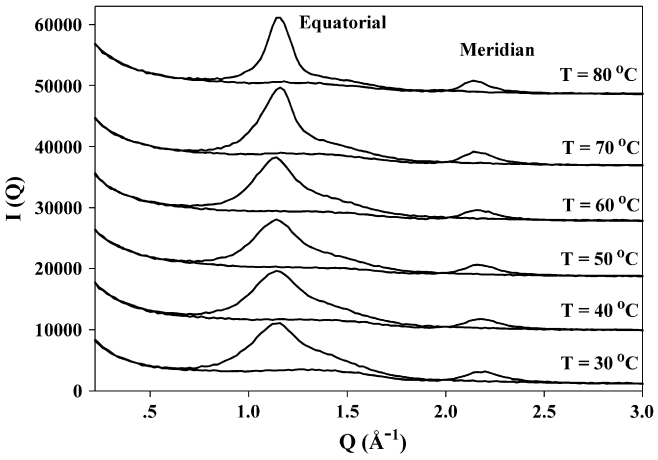

Fig. 6. The scattering intensity profiles in equatorial and meridional sections of the block terpolymer fibres at various conditions of processing which correspond to Fig. 5.

varies from fibre to fibre in a fairly systematic manner. These spherical harmonic components $I_{2n}(|\underline{Q}|)$ obtained can be used to evaluate the corresponding orientation parameters, $\langle P_{2n}(\cos\alpha)\rangle_D$ from Ref. [17]:

$$\langle P_{2n}(\cos\alpha)\rangle = \frac{I_{2n}(|\underline{Q}|)}{(4n+1)I_0(|\underline{Q}|)P^0_{2n}(\cos\alpha)} \quad (5)$$

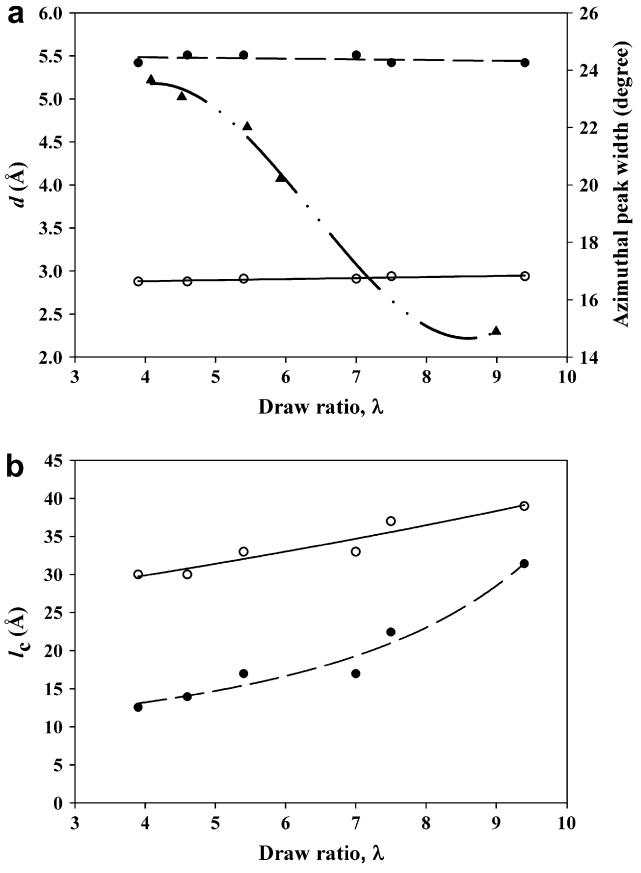

Fig. 7. (a) Plot of interplanar distances taken from the equatorial (●) and meridional (○) sections shown in Fig. 6 against the draw ratio employed in their preparation together with the peak width (▲) displayed in the azimuthal sections shown in Fig. 8 for the same fibres; (b) plot of crystal size measured in the fibre direction (○) and perpendicular to the fibre axis (●) against the draw ratio for each of the block terpolymer fibers. Full draw conditions are given in Table 1.

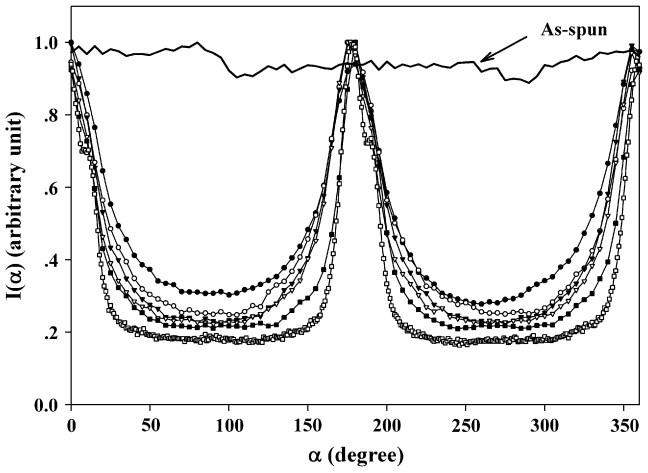

Fig. 8. Azimuthal sections of the scattering patterns of the as-spun and drawn fibres of the block terpolymer at a $Q = 1.16$ Å^{-1}: —: as-spun; ●: $\lambda = 3.9$ Å; ○: $\lambda = 4.6$ Å; ▼: $\lambda = 5.4$ Å, ▽: $\lambda = 7.0$ Å; ■: $\lambda = 7.5$ Å, □: $\lambda = 9.4$ Å (full draw conditions are given in Table 1).

where $P^0_{2n}(\cos\alpha)$ are the amplitudes of the harmonics for a model representing perfect alignment of the structural units, for example crystalline planes. Although X-ray scattering gives access to the full orientation distribution or in terms of the spherical harmonics, the amplitudes which represent the orientation distribution, attention is often focused on the first term $\langle P_2(\cos\alpha)\rangle$ and in a polymer context this is sometimes referred to as the Hermans Orientation Function. For the case of an equatorial crystal reflection in which the scattering for the perfectly aligned systems is confined to the equatorial plane, $P^0_2(\cos\alpha) = -0.5$ [17].

We have applied this approach to the spherical harmonics shown in Fig. 9 to calculate the values of $\langle P_2(\cos\alpha)\rangle$ corresponding to the equatorial peak at $|\underline{Q}| \sim 1.16$ Å^{-1} and the results are plotted in Fig. 10 against the draw ratio used to prepare each fibre. The uncertainty in these values is of the order of 0.02. The as-spun fibre is essentially isotropic and so $\langle P_2(\cos\alpha)\rangle \sim 0$. Thus there is a step up in orientation from the as-spun fibre to that prepared with a draw ratio of $\lambda = 3.9$ Å. There is what appears to be a plateau in the orientation versus draw ratio curve of 0.2–0.3 until a turn up at the highest draw ratio leads to a doubling of the orientation parameter. The levels of anisotropy of the crystal and amorphous components will impact differently on the mechanical properties and it is very useful to separate out the effects. As these are rather complicated materials with blocks of differing composition and monomer sequence, the separation is not as straightforward as for a highly crystalline polymer. The problem can be easily understood by inspecting the azimuthal sections in Fig. 8.

3.4. Orientation of crystalline component

We have developed a novel approach to the separation of the crystalline and amorphous components for this work. In particular, this approach allows us to identify in an unambiguous manner the features in the scattering which arises from a particular component. For the purpose of presenting the approach we consider a two phase system containing a fraction x of crystalline polymer and $1-x$ of amorphous polymer although the method can be extended to any number of components. For a system in which the length scale of the domain size of the two phases is large compared with the length scale giving rise to the scattering, the total scattering $I(|\underline{Q}|,\alpha)$ can be written as the algebraic sum of the scattering from the two components:

$$I(|\underline{Q}|,\alpha) = xI^c(|\underline{Q}|,\alpha) + (1-x)I^a(|\underline{Q}|,\alpha) \quad (6)$$

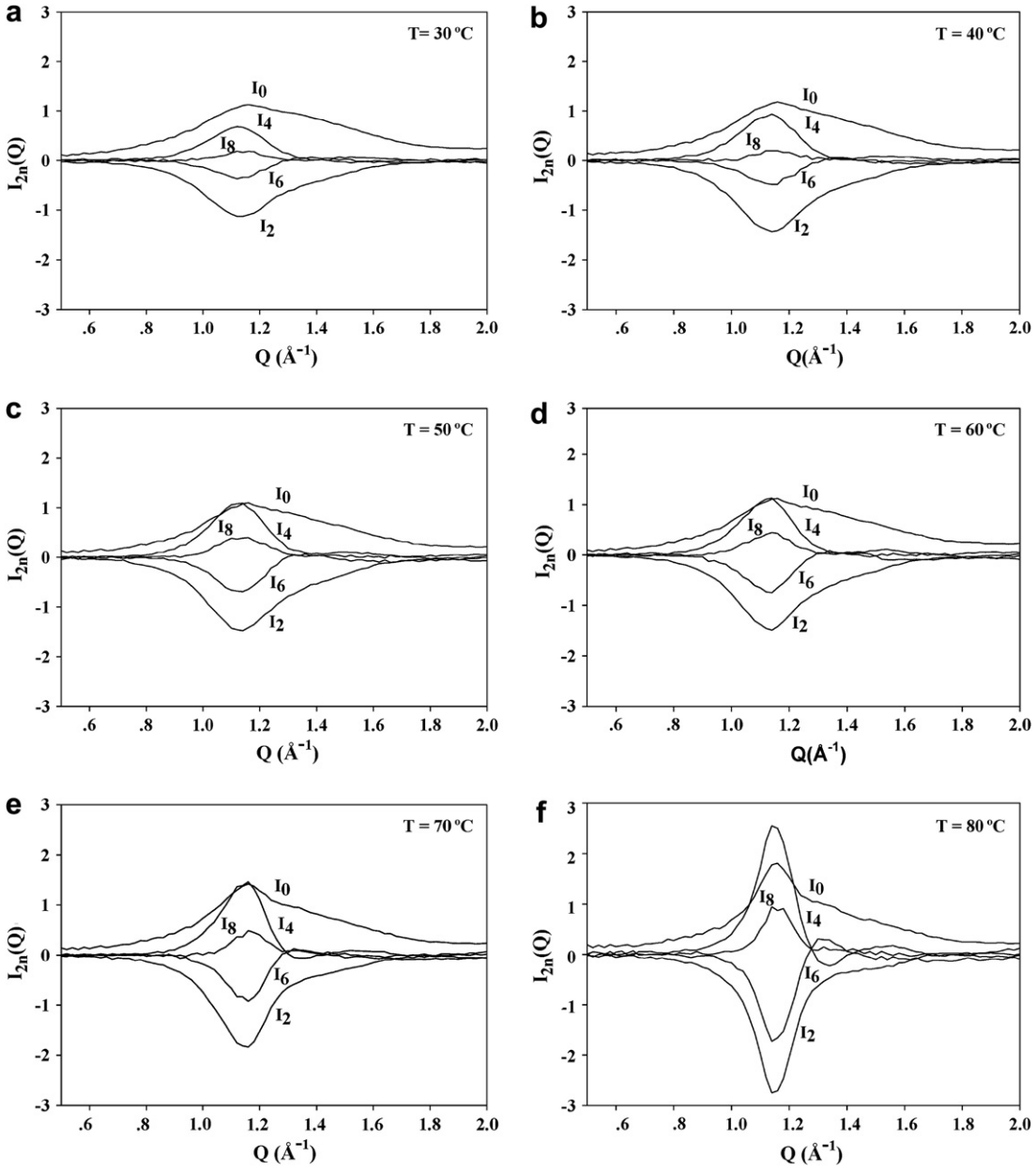

Fig. 9. Profiles of the first five spherical harmonic components calculated from the scattering data for each pattern of the block terpolymer fibre in Fig. 5.

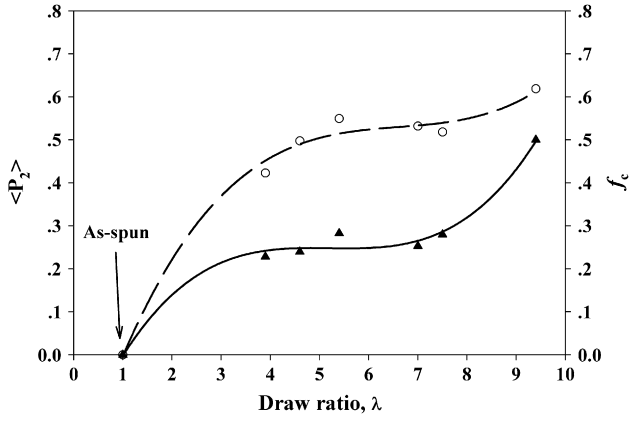

Fig. 10. Overall orientation (▲) and fraction of oriented crystals (○) as a function of draw ratio for the terpolymer drawn fibres (full draw conditions are given in Table 1).

The orthogonal nature of the spherical harmonics described above means that for a two phase structure in which the scattering is additive, the resultant spherical harmonics will also be linear combinations of the harmonic functions for each phase. We can write [18]:

$$I_{2n}(|\underline{Q}|) = xI^{c}_{2n}(|\underline{Q}|) + (1-x)I^{a}_{2n}(|\underline{Q}|) \quad (7)$$

where $I^{c}_{2n}(|\underline{Q}|)$ are the spherical harmonics for the crystalline phase and similarly $I^{a}_{2n}(|\underline{Q}|)$ for the amorphous phase.

The strength of a particular spherical harmonic term at a fixed value of $|\underline{Q}|$ depends upon three specific factors. The first dependence involves the details of the spherical harmonic function which depends in turn on the structure giving rise to the scattering. For samples with the same structure, the harmonic term will have the same form, i.e. peak positions, peak shapes and relative peak heights. The second factor is the composition and there is a simple linear relation with the fraction of that phase. The third factor is the

level of preferred orientation. The second and third terms are simple multipliers and do not depend upon the value of $|\underline{Q}|$. We can express this sensitivity of the spherical harmonics on the level of preferred orientation by expanding Eq. (7) as:

$$I_{2n}(|\underline{Q}|) = xI_{2n}^{0c}(|\underline{Q}|)D_{2n}^{c}\frac{2\pi}{4n+1} + (1-x)I_{2n}^{0a}(|\underline{Q}|)D_{2n}^{a}\frac{2\pi}{4n+1} \quad (8)$$

where $I_{2n}^{0c}(|\underline{Q}|)$ are the functions for the pure perfectly aligned crystalline phases and $I_{2n}^{0a}(|\underline{Q}|)$ are the equivalent functions for the amorphous phase and D_{2n}^{c} and D_{2n}^{a} are coefficients describing the orientation distribution functions $D^{c}(\alpha)$ and $D^{a}(\alpha)$ for the crystal and amorphous components, respectively.

For a particular experimentally observed harmonic Eq. (8) reduces to:

$$I_{2n}(|\underline{Q}|) = k_{2n}^{c}I_{2n}^{0c}(|\underline{Q}|) + k_{2n}^{a}I_{2n}^{0a}(|\underline{Q}|) \quad (9)$$

where k^{c} and k^{a} are scaling constants for the crystalline and amorphous phases, respectively, with k^{c} for the crystalline phase given by

$$k_{2n}^{c} = xD_{2n}^{c}\frac{2\pi}{4n+1} \quad (10)$$

and k^{a} for the amorphous phase by a similar expression. Eq. (9) provides a route to the separation of the scattering into the contributions from each phase. Essentially, each observed spherical harmonic is made up of the sum of the harmonics of the same order for the crystalline and amorphous components within the sample weighted in a simple multiplicative manner by a factor which depends on the level of orientation and the composition. Eq. (9) makes clear that to observe a non-zero value of a spherical harmonic at a particular value or range of $(|\underline{Q}|)$, three conditions must be met, the value of $I_{2n}^{0a}(|\underline{Q}|)$ for the pure perfectly aligned phase must be non-zero, the composition must be non-zero and the value of the orientation parameter D_{2n} must be non-zero. If any one of these factors is zero, the observed harmonic will be zero. We will exploit the latter condition to separate out the crystalline component from the rest of the scattering.

Although we write the scattering pattern or the orientation distribution function as the sum of an infinite series of spherical harmonics (Eq. (4)), from a practical perspective often only the first few terms are non-zero. To illustrate this we have utilized as a model orientation distribution function, the expression shown below:

$$D(\alpha) = \cos^{k}\alpha \quad (11)$$

Fig. 11 shows three representative normalized plots of $D(\alpha)$ against α with $k = 1$, 3 and 8. The corresponding orientation parameters calculated for this distribution are shown in Table 2. For $k = 1$ with a very broad distribution function only $\langle P_2\rangle$ has a significantly non-zero value, while for $k = 3$ only $\langle P_2\rangle$ and $\langle P_4\rangle$ are non-zero. With $k = 8$, the orientation function is now quite sharp and is approaching that shown by the crystals. The values of $\langle P_2\rangle$, $\langle P_4\rangle$, $\langle P_6\rangle$ and $\langle P_8\rangle$ are now all non-zero, although the magnitude of the values drop off considerably with the order of the harmonic.

For the amorphous phase, we can anticipate a relatively low level of preferred orientation and hence we can expect that only $\langle P_2\rangle$ and possibly $\langle P_4\rangle$ will be non-zero [19]. As a consequence only I_2 and possibly I_4 will contain a non-zero amorphous contribution. We can return to the plots of the spherical harmonics shown in Fig. 9 and review the variation in peak shapes highlighted earlier.

Looking again at Fig. 9e, we can see that the higher order harmonics, I_6 and I_8 have a similar shape as does I_4. In other words, each of these harmonics contains a contribution from the same structure. We attribute this sharp (in terms of $|\underline{Q}|$) peak to the crystal reflection. There appears to be no amorphous contribution towards this peak in-line with expectations that the higher order orientation parameters for the amorphous phase are close to zero. Clearly this sharp feature appropriately scaled must be also present in I_2. Indeed, inspection of the plots shows that I_2 does contain at least one other component. If we continue the comparisons, the broad nature of I_0 stretching way beyond the features in I_2 reveals that there is a further structural component which is only present in an isotropic form. We assign these three structures as crystalline, oriented or ordered amorphous and an isotropic highly disordered component which appears to be unaffected by the drawing process.

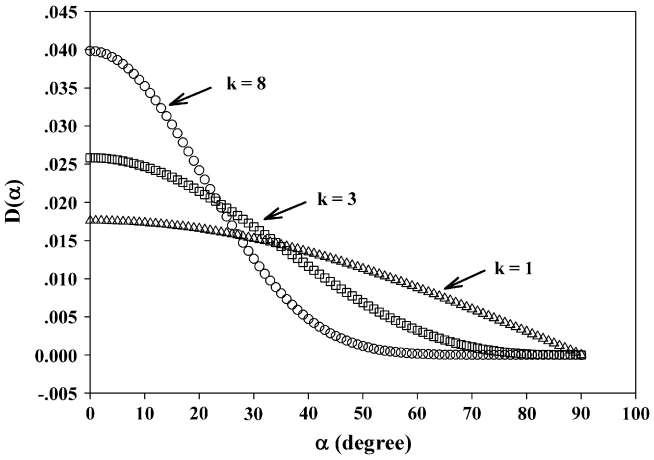

Fig. 11. A plot of a simulated orientation distribution function $D(\alpha)$ described in the text.

From the analysis presented above, it is reasonable to select the sharp peak in I_8 as representing the component which only arises from the crystalline phase, while I_2 contains components from both the amorphous and crystalline phases. In fact, I_2, is the linear sum of the equivalent harmonics for the crystalline and amorphous components (Eq. (9)). As we have a good appreciation of the form of the amorphous phase we can obtain a fit by adjusting a scaling parameter b to numerically fit I_2 using bI_8 where we judge the efficacy of the fit by examination of the residue of $I_2 - bI_8$ and comparing this to the expected curve. The fact that the amorphous peak will be broad with a single maximum considerably facilitates this approach. The profiles of I_2, bI_8 and $I_2 - bI_8$ as a function of $|\underline{Q}|$ for the series block terpolymer fibres are shown in Fig. 12. For convenience of display we have multiplied each function by -1 to invert the curves. Note that the peak shape for the oriented amorphous is similar for the different draw temperatures revealing that the basic oriented amorphous structure remains constant for different drawing temperatures.

If I_2 is considered as the total contribution, the fraction of the oriented component can be calculated as below.

$$f_{\text{crystal}} = \int_{Q_{\min}}^{Q_{\max}} \frac{bI_8(|\underline{Q}|)}{I_2(|\underline{Q}|)}\mathrm{d}Q$$

Table 2
Orientation parameter calculated for an orientation distribution $D(\alpha) = \cos^{k}\alpha$ for specific values of the simple scalar k

k	$\langle P_2\rangle$	$\langle P_4\rangle$	$\langle P_6\rangle$	$\langle P_8\rangle$
1	0.25	<0.01	<0.01	<0.01
3	0.50	0.06	<0.01	<0.01
8	0.73	0.34	0.09	0.01

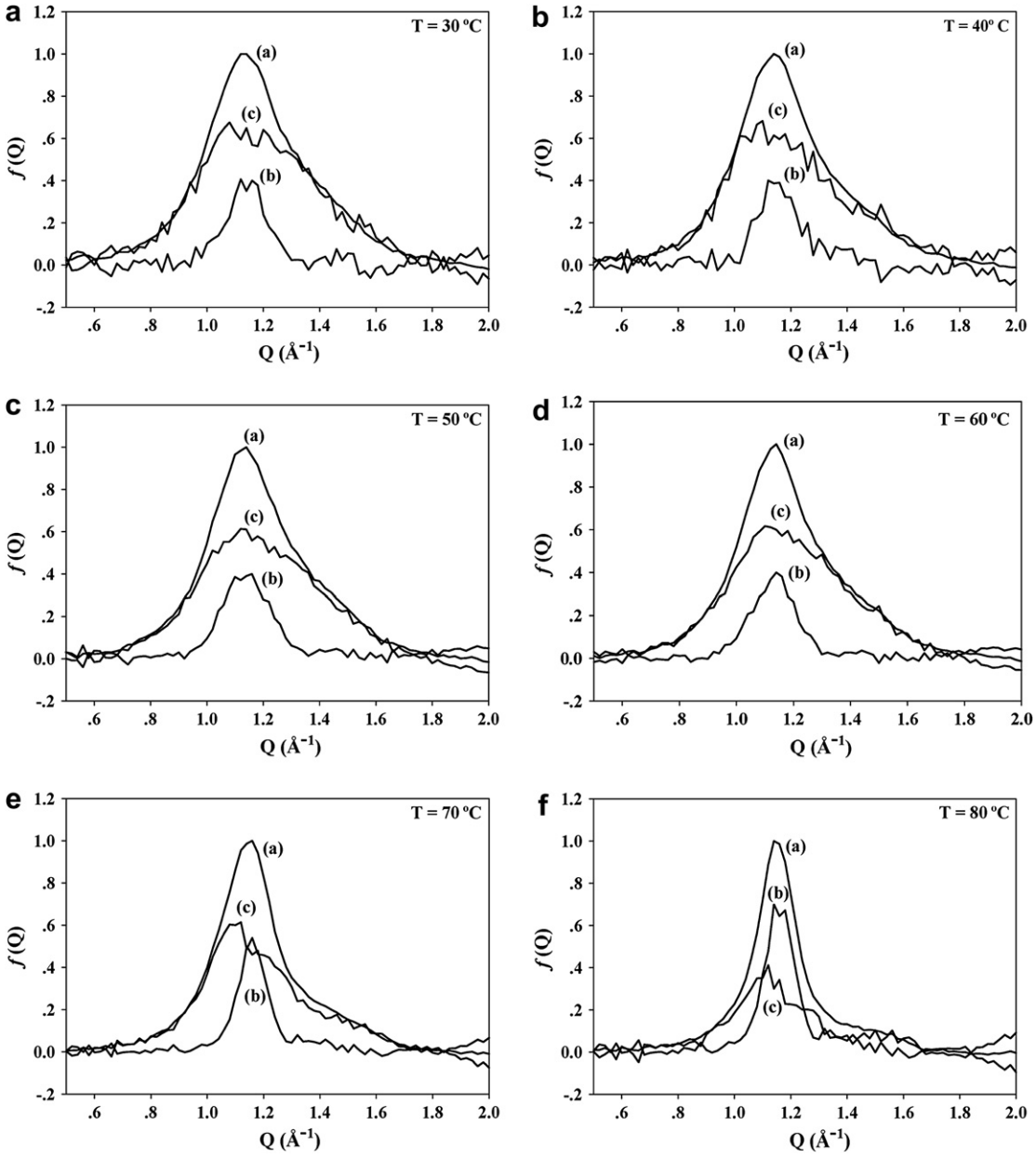

Fig. 12. Profiles of spherical harmonic components as a function of$Q$ for the block terpolymer fibre (a) $-I_2$ (b) $-bI_8$ (c) $-(I_2 - bI_8)$ where b is a fitting constant obtained in the analysis (see text).

In these fibres, the crystal orientation is relatively high, i.e. D^{c}_{2n} approaches unity, and consideration of Eqs. (9) and (10) reveals that for high crystal orientations, the fraction calculated is essentially equivalent to the fraction of crystalline material which is anisotropic. Fig. 10 shows a plot of f_{crystal} calculated in this manner as a function of draw ratio for drawn fibres under various draw conditions. As can be seen in Fig. 10, after the initial step up from the zero value for the as-spun fibre, the value of f_{crystal} remains largely constant until the draw ratio exceeds 7.5 or probably more significantly the temperature exceeds 70 °C. The overriding advantage of this technique based on an analysis using spherical harmonics is that we identify the crystal component without recourse to the ambiguity of fitting somewhat arbitary peak shape functions. The information for differentiating between the components comes directly from the data itself. The fraction of oriented crystals mirrors the increase in overall crystallinity measured using DSC shown in Fig. 4.

3.5. Small-angle X-Ray scattering

The SAXS patterns of as-spun and drawn fibres are shown in Fig. 13. The dark square in the center is the shadow of the beam stop. The as-spun fibre (Fig. 13a) shows no distinctive small-angle X-ray scattering pattern characteristic of a microphase separated structure. This suggests that the terpolymer system exhibits the disordered state as might be expected on the basis of the distribution of block lengths and intrablock sequences. The as-spun fibre exhibits a strong equatorial streak typical of microvoids or of a microfibrillar structure [20]. The anisotropic nature of the scattering and the amorphous state of the as-spun fibre suggests that these are voids which have been extended during the fibre spinning process. Subsequent drawing of the as-spun fibres further extends these voids as can be observed in the increasing level of anisotropy in this scattering and in particular through the reducing width of the streak in the vertical direction.

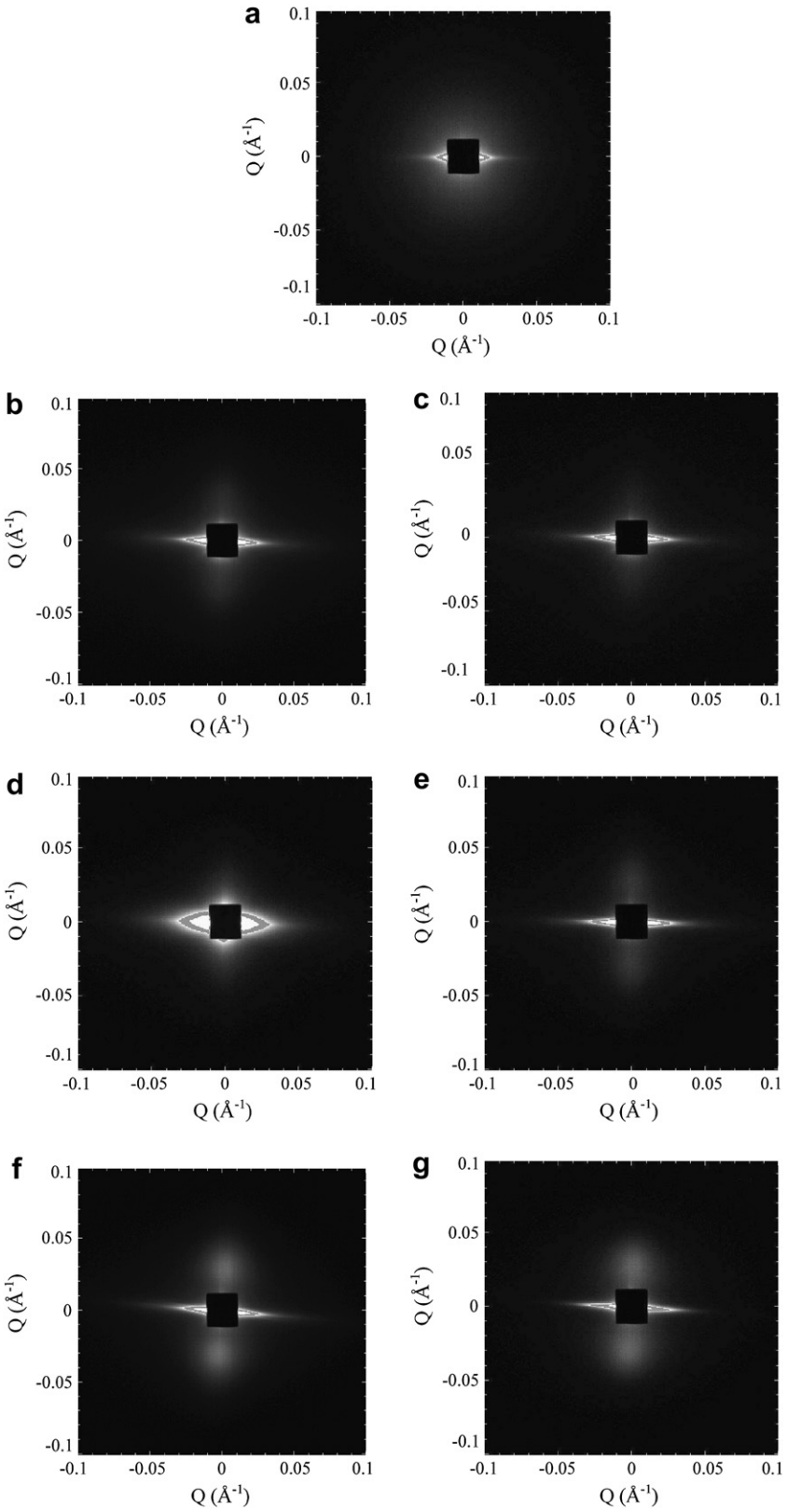

Fig. 13. SAXS patterns of the block terpolymer fibers drawn at various conditions – see Fig. 5 for key.

Fibres drawn at 30, 40 and 50 °C do not exhibit any additional features. Fibres drawn at higher temperatures show an additional meridional scattering which becomes most intense for the pattern recorded for the sample drawn at 80 °C. The so-called two point pattern is routinely found in highly drawn semi-crystalline fibres and shows that the thin crystal lamellar are formed perpendicular to the fibre axis. The SAXS patterns are highly anisotropic and indicate a high level of preferred orientation of the crystal lamellae as was anticipated from the almost perfect alignment of the crystal planes exhibited in the WAXS patterns (Fig. 5). For the patterns

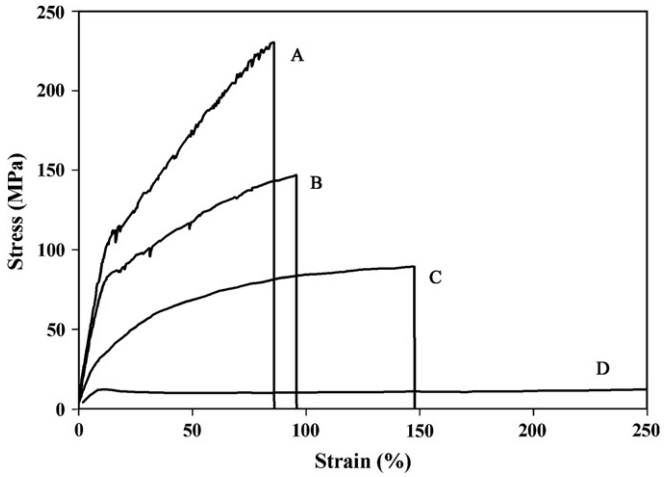

Fig. 14. Stress–strain curves recorded for drawn fibres prepared at 70 °C (A), 50 °C (B) and 30 °C (C) using the conditions recorded in Table 1 and the as-spun fibre (*D*). Note that the strain axis is truncated in the case of the as-spun fibre.

obtained from samples prepared at 70 and 80 °C, the peaks of the broad meridional maxima occur at 0.029 $Å^{-1}$ and 0.027 $Å^{-1}$ giving a long periods of 217 and 233 Å and hence lamellar thicknesses of ~60 Å. These compare with the crystal thicknesses of ~40 Å derived from the wide-angle scattering where the apparent peak width will also be influenced by crystallographic defects and strain. An alternative explanation is the presence of an ordered amorphous interface region.

3.6. Mechanical properties

Stress–strain curves for each set of fibres were obtained using the procedure outlined in Section 3.3. Representative stress–strain curves are shown in Fig. 14 and these illustrate the marked increase in modulus and reduction in elongation at failure as the temperature employed in the hot drawing of the fibres is increased. These curves were used to derive the mechanical properties particularly significant to surgical sutures, namely, the initial modulus, the tensile strength and the elongation at failure and these extracted properties are shown in Fig. 15–17. The as-spun fibre is an isotropic amorphous material which is highly elastic. It is characterized by a low tensile strength (<20 MPa), a high elongation at break (>1400%, note the strain scale in Fig. 14 has been truncated) and

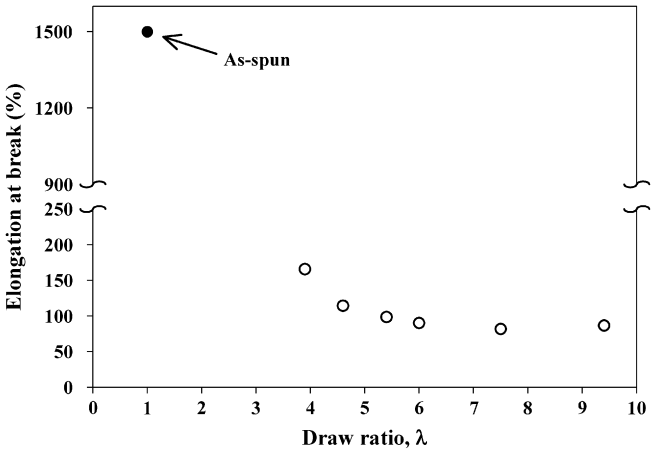

Fig. 16. Elongation at break of as-spun fibre and drawn fibres.

a low Young's modulus. These features are typical of an unoriented amorphous system close to the glass transition. Such a material is very unsuited to use as a surgical suture. The mechanical properties of fibres were much improved after hot drawing with tensile strengths of >70 MPa, elongations at break of <200% and Young's moduli of >300 MPa. The extent of the enhancement largely depended upon the conditions employed for the drawing. Fig. 15 shows the tensile strength as a function of draw ratio. As can be seen, the higher the draw ratio, the stronger the fibre, although this is not the case for the fibres drawn at the highest temperature. The plot of the modulus against the draw ratio used in the preparation largely mirrors the tensile strength plot. The extension ratio at failure reduces significantly on hot drawing and reaches a plateau of about 100% for the strongest fibres. In terms of application as a surgical suture, the 80 °C fibre exhibits a modulus comparable to current medical practice, but the strength is below that of equivalent sutures prepared from homopolymers such as the PDSII suture with a strength ~500 MPa and an extension at failure of over 200%. WAXS/SAXS patterns of the PDSII suture show that it exhibits a highly aligned crystal structure with a well defined lamellar crystal morphology.

The variation of the strength of the fibres does not only relate to the molecular organization in the fibre but also to the microscopic morphology. The presence of defects arising during the two-stage processing route may lead to premature failure. Wu et al. [21] and Ran et al. [22] have reported that drawing at high rates may lead to

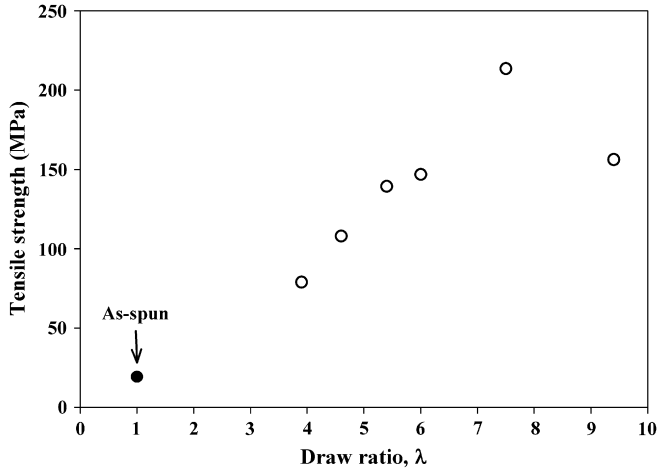

Fig. 15. Tensile strength of as-spun and drawn fibres.

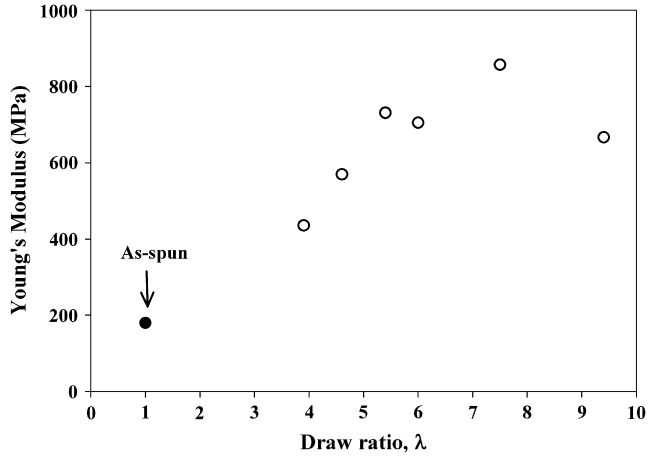

Fig. 17. Young's moduli of as-spun fibre and drawn fibres.

a greater level of defects. The small-angle scattering reveals the presence of microvoids which may initiate premature breakage. It may be that the strength of the terpolymer is limited by defects introduced in the two-stage batch process and that a continuous process would lead to enhanced strength and extensibility. However, we attribute the reduced strength of the 80 °C fibre to the relatively lower draw rate used in its preparation and this is discussed below.

4. Discussion

The WAXS and SAXS measurements show that the as-spun filaments are amorphous and isotropic and there is no evidence for a phase separated morphology arising from the block nature of the polymer structure. Hot drawing of these filaments leads to anisotropic structures with a significantly enhanced modulus and strength. This hot drawing leads to the development of small crystals which are highly aligned with respect to the drawing direction. There is a substantial amorphous component which is oriented. The overall anisotropy in the scattering remains largely constant except at the highest draw ratio but there is a steady increase in the fraction of the oriented material which is crystalline. There is a substantial fraction of the material which remains isotropic and which appears to be unaffected by the drawing which in considerable part must reflect the statistical nature of the terpolymer blocks.

Crystallisation in block copolymers is an area of topical interest, for example the review of Loo and Register [23]. A variety of novel behaviours have been identified in block copolymer systems with well defined close to monodisperse blocks in which there is a competition between crystallisation and microphase segregation. Where the interblock segregation is sufficiently strong, crystallisation may be contained within a microdomain even where the confining matrix is liquid-like. In the system considered in this work, there is no evidence for phase segregation in the melt, as might be expected from the more polydisperse nature of the blocks and the expected weak interaction parameter of the blocks based on the observations of copolymers of lactide and caprolactone [24]. As a consequence, crystallisation proceeds from a disordered melt state.

Hot drawing is a complex matter with numerous parameters and influences. As the draw temperatures used are very close to the glass transition, the temperature will have a major impact on the dynamics of the amorphous as-spun filament. By drawing at the maximum rate possible for a given temperature we are attempting to automatically compensate for the increase in mobility. Of course this does not eliminate the influence of the increasing draw ratio (Table 1) and the changing crystallization conditions. A striking aspect of this study is how the features of crystallization from an anisotropic state, such as the enhancement of crystallinity with drawing (Fig. 4) and the almost perfect alignment of the crystals induced (Fig. 5), parallel those shown by the homopolymer of polylactide [15] and other homopolymers despite the rather complex nature of the terpolymer and the constituent blocks.

As the crystals which form are small, both in terms of size and fraction, we might expect that these have a smaller contribution to the overall modulus than the alignment of the amorphous component. However, the development of a preferred alignment of the amorphous component requires an increasing draw rate as the temperature increases to compensate for the higher level of molecular mobility. The fact that the fibre drawn at 80 °C is not the stiffest or strongest from the series considered here reflects the fact that it was only possible to use a relatively slow draw rate. Extrapolation of the draw rates used over the range 30–70–80 °C gives a value ~8000%/min rather than the value of 4480%/min used. As a consequence there is a marked reduction in the level amorphous orientation as can be seen in Figs. 5g and 12f which has a major impact of the mechanical properties. The effects are partially masked by the substantial increase in the fraction of crystal orientation. We anticipate that a fibre drawn at the required rate at 80 °C would develop enhanced mechanical properties. To achieve this requires an increase in molecular weight of the terpolymer. The level of crystallinity which is reached appears to be close to the statistical limit and it may be possible to achieve the considerable increase in oriented crystal fraction at a lower processing temperature if the amount of glycolide in the terminal blocks was reduced slightly. This would provide an even lower process temperature which would lead to fibres with even greater chemical stability and higher levels of purity. The latter is particularly important for materials intended for medical applications. However, the limit on the level of crystallinity through the statistical nature of the terminal blocks does provide an enhanced flexibility which is essential for knot integrity in suture applications especially for smooth monofilaments. In summary, the fibre should be drawn at as high a rate as possible at a particular temperature to induce high molecular orientation along the fibre axis with a moderate level of crystallinity to help stability. The block nature of the terpolymer provides an excellent framework to achieve these different aims.

It is interesting to note that although the level of oriented crystalline material is largely constant from 30 to 60 °C, the SAXS patterns only show significant features at the higher temperatures. We attribute this to the limited contrast of the system due to the similarities of the amorphous and crystal densities and the increased contrast in the higher temperature fibres due to the considerable difference in the differential thermal expansion of the two components as these are essentially quenched samples.

5. Conclusions

The two-stage processing route proposed for this biodegradable terpolymer has proved to be an effective approach to the generation of absorbable monofilament sutures. It offers a relatively low process temperature and subsequent gains in stability and purity of the final filament. The design of the material provides the framework for generating materials with the required properties. Although the statistical nature of the blocks allows low temperature processing it is still necessary to draw at 80 °C to achieve the maximum crystallization during the draw time. Increasing the molecular weight or slightly reducing the gylcolide content in the terminal blocks provides two attractive options for enhancing even further the mechanical properties. The methodology introduced for separating the scattering into the differing structural components clearly has wide application and the results provide interesting input to the wider theme of stress-induced crystallization.

Acknowledgements

The authors gratefully acknowledge the Faculty of Science, Chiang Mai University and the National Metal and Materials Technology Center of Thailand (MTEC) for supportable this work. WC is also indebted for financial support by Thai Ministry of University Affair and the Graduate School of Chiang Mai University. The small-angle X-ray scattering was performed at the CCLRC Daresbury Synchrotron Facility (UK) and the authors thank the beam-line scientist Anthony Gleeson for his assistance with the experiments.

References

[1] Shalaby SW, Burg KJL. Absorbable and biodegradable polymers (advances in polymeric biomaterials). CRC; 2003.
[2] Wise DL, Trantolo DJ, Altobelli DE, Yaszenski MJ, Gresser JD, Schwartz ER, editors. Encyclopedic handbook of biomaterials and bioengineering part A: materials, vol. 1. New York: Marcel Dekker, Inc; 1995.

[3] Uhrich KE, Cannizzario SM, Langer RS, Shakesheff KM. Chem Rev 1999;99:3181–98.
[4] Vert M. Biomacromolecules 2005;6:538–46.
[5] Bezwada RS, Jamiolkowski DD, In-Young L, Agarwal V, Persivale J, Trenka-Benthin S, et al. Biomaterials 1995;16:1141–8.
[6] Baimark Y, Molloy R, Molloy N, Siripitayananon J, Punyodom W, Sriyai M. J Mater Sci Mater Med 2005;16:699–707.
[7] Channuan W, Siripitayananon J, Molloy R, Sriyai M, Davis FJ, Mitchell GR. Polymer 2005;46:6411–28.
[8] Srisa-Ard M, Molloy R, Molloy N, Siripitayananon J, Sriyai M. Polym Int 2001;50:891–6.
[9] Baimark Y, Molloy R. Polym Adv Technol 2005;16:332–6.
[10] Walczak ZK. Processes of fibre formation. Elsevier; 2002.
[11] Mitchell GR. In: Allen G, Bevington J, editors. Comprehensive polymer science. New York: Pergamon Press; 1989. p. 687–729.
[12] Gupta B, Revagade N, Hilborm J. Prog Polym Sci 2007;32:455–82.
[13] Turner JF, Riga A, O'Connor A, Zhang J, Collis J. J Thermal Anal Cal 2004;75: 257–68.
[14] Mitchell GR. Polymer 1984;25:1562–72.
[15] Mahendrasingam A, Blundell DJ, Parton M, Wright AK, Rasburn J, Narayanan T, et al. Polymer 2005;46:6009–15.
[16] Fu XB, Hsiao BS, Chen G, Zhou J, Koyfman I, Jamiolkowski DD, et al. Polymer 2002;43:5527–34.
[17] Lovell R, Mitchell GR. Acta Crystallogr 1981;A37:135.
[18] Mitchell GR, Saengsuwan S, Bualek-Limcharoen S. Prog Colloid Polym Sci 2005;130:149–59.
[19] Mitchell GR, Brown DJ, Windle AH. Polymer 1985;26:1755–62.
[20] Murthy NS. In: Salem DR, editor. Structure formation in polymeric fibres. Munich: Carl Hanser Verlag; 2001. p. 475–91.
[21] Wu J, Schultz JM, Samon JM, Pangelinan AB, Chuah HH. Polymer 2001;42:7161–70.
[22] Ran S, Fang D, Zong X, Hsiao BS, Chu B, Cunniff PM. Polymer 2001;42:1601–12.
[23] Loo Y-L, Register RA. In: Hamley IW, editor. Developments in block copolymer science and technology. London: Wiley; 2004. p. 213–43 [chapter 6].
[24] Hamley IW, Castelletto V, Castillo RV, Muller AJ, Martin CM, Pollet E, et al. Macromolecules 2005;38:463–72.